Journal of Science and Technology in Civil Engineering, HUCE, 2024, 18 (4): 69–82

DYNAMIC ANALYSIS OF CARBON NANOTUBE-REINFORCED COMPOSITE PLATES USING REDUCED ORDER ISOGEOMETRIC MODEL

Van Hai Luong[a,b,*], Qui X. Lieu[a,b]

[a]*Faculty of Civil Engineering, Ho Chi Minh City University of Technology (HCMUT), 268 Ly Thuong Kiet street, Ward 14, District 10, Ho Chi Minh city, Vietnam*
[b]*Vietnam National University Ho Chi Minh City (VNU-HCM), Linh Trung ward, Thu Duc city, Ho Chi Minh city, Vietnam*

Article history:
Received 07/8/2024, Revised 10/9/2024, Accepted 23/9/2024

Abstract

In this work, a reduced order isogeometric model is proposed to analyze the dynamic behavior of carbon nanotube-reinforced composite plates. In which, the mechanical properties of the material are functionally graded through the plate thickness employing four distributions of carbon nanotubes. A third-order shear deformation theory is employed to represent the displacement along with the plate thickness, whilst a non-uniform rational B-splines surface is utilized to approximate the displacement in the plate plane. The dynamic responses at important degrees of freedom are resolved by the Newmark method instead of dealing with all degrees of freedom as those of the full model. Accordingly, a reduced order model based on the second-order Neumann series expansion is utilized to build the isogeometric analysis. Several examples are tested to illustrate the ability of the suggested paradigm. Obtained outcomes are compared with those of other works and full model to prove the reliability of the reduced Isogeometric analysis.

Keywords: dynamic analysis; carbon nanotube-reinforced composite (CNTRC) plates; isogeometric analysis (IGA); reduced order model (ROM).

https://doi.org/10.31814/stce.huce2024-18(4)-06

1. Introduction

In the past few decades, advanced composite materials have extensively attracted a large number of scholars in the scientific community. This discovery is known as a new revolution, especially in material science and structural engineering. Among them, carbon nanotube-reinforced composite (CNTRC) is one of the notable materials owing to its prominent thermo-mechanical properties such as high stiffness, high strength, light weight, and so on. For those reasons, carbon nanotubes (CNTs) are often integrated into conventional material matrices such as isotropic polymer to produce advanced materials with more outstanding features, aiming at designing structural members in many fields such as automotive, aerospace, civil engineering, etc. Therefore, studying the mechanical behavior of structural components such as beam [1], plate [2, 3], and shell [4] is essential and crucial, especially for cases under free vibration, time-history loads, etc. With this aspect, interesting readerships can consult a review paper reported by Soni et al. [5] for more comprehensive discussions.

In 2005, Hughes et al. [6] first introduced an enhanced numerical approach as a competition and alternative to the standard finite element method (FEM) which is the so-called isogeometric analysis (IGA). This technique serves as a bridge for integrating computer-aided design (CAD) and finite element analysis (FEA) into a unified model, aiming to reduce the computational cost. This IGA utilizes

*Corresponding author. *E-mail address:* lvhai@hcmut.edu.vn (Luong, V. H.)

the same non-uniform rational B-spline (NURBS) for both geometrical modeling and mechanical behavior analysis. Hence, any complicated geometrical domains can be also exactly represented, whilst high-order derivatives and continuities required to simulate the responses of composite materials can be naturally guaranteed, especially for CNTRC plates [7, 8], functionally graded (FG) porous plates [9], FG plates [10]. The IGA's applications could be also found in the following publications [11–14].

Nevertheless, all the above-mentioned researches have analyzed the dynamic behavior of CNTRC plates within the full IGA framework. This means that all degrees of freedom (DOFs) defined at control points of the structural system after discretizing by the IGA context in the algebraic dynamic equation system are resolved. Nevertheless, for issues encountered in structural health monitoring (SHM), especially when measurement sensors are limited, the way of analyzing such problems in the SHM by the full model is not suitable. More concretely, in such cases, the signals at important DOFs of a monitored structure are measured by sensors. Then, the information of the remaining DOFs that are not recorded by sensors is numerically inferred by the mathematical equations formulated from the so-called model order reduction (MOR) or reduced order model (ROM). With this regard, studies on the applications of MOR can be found in the literature. In particular, Dang et al. [15] built ROMs for the linear time-history analysis for damage detection of truss structures via inverse optimization. Qui [16] applied the MOR technique to infer time-dependent signals at unmeasured DOFs, serving the calculation of the acceleration-displacement-based strain energy indicator (ADSEI). Moreover, Qui [17] utilized the second-order Neumann series [18] to compute the free vibration data at unmeasured DOFs.

To the best knowledge of the author, for such problems, there have been no such reports on applying the IGA framework to the dynamic analysis of CNTRC plates. Therefore, this work is conducted as the first contribution. Following the content and scope of this study. The next Section presents the theoretical basis for CNTRC plates. Moreover, the governing equations of motion for dynamic analysis by the IGA based on the four-variable plate theory are also reported. Section 3 derived the reduced IGA based on second-order Neumann series expansion. Section 4 tests several examples to prove the reliability of the proposed paradigm. Finally, several crucial conclusions are drawn.

2. Theoretical basis

2.1. Carbon nanotube-reinforced composite material

As depicted in Fig. 1, four types of CNT distributions through the thickness of CNTRC plate (h) are taken into account in this work. It is noted all CNTs are only arranged parallel to the x-axis. More concretely, if the distribution of CNTs is uniform, it is called as UD. The remaining three types of CNT distributions are known as V, O and X. More concretely, the V type possesses CNTs-rich at the top surface of CNTRC plate. The mid-plane of the CNTRC plate is CNTs-rich in the case of O type. Finally, the X configuration is of the CNTs-rich at both top and bottom surfaces. The distribution of CNT volume fractions through the plate thickness for such four types are defined as follows [2]

$$V_{CNT}(z) = \begin{cases} V^*_{CNT}, & \text{U} \\ \left(1 + \dfrac{2z}{h}\right) V^*_{CNT}, & \text{V} \\ 2\left(1 - \dfrac{2|z|}{h}\right) V^*_{CNT}, & \text{O} \\ 2\left(\dfrac{2|z|}{h}\right) V^*_{CNT}, & \text{X} \end{cases} \tag{1}$$

where

$$V_{CNT}^{*} = \frac{w_{CNT}}{w_{CNT} + (\rho_{CNT}/\rho_m) - (\rho_{CNT}/\rho_m)\, w_{CNT}} \tag{2}$$

in which w_{CNT} is the mass fraction of CNTs; ρ_{CNT} and ρ_m are the densities of the CNTs and the polymer matrix, respectively.

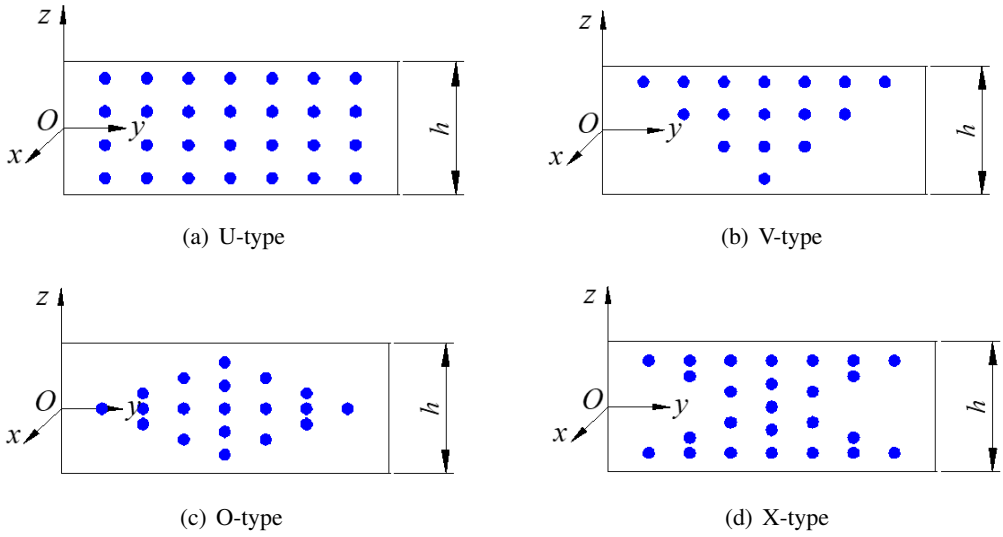

(a) U-type (b) V-type

(c) O-type (d) X-type

Figure 1. Four types of CNT distributions

As known, the CNTRC materials are often made of two distinct constituents as a mixture of CNTs (fiber) and isotropic polymer (matrix), the effective material properties are thus required to be estimated. Since the simplicity and accuracy of the rule of mixtures, the strategy is adopted in this work. Accordingly, the effective material properties of CNTRC plate are given as follows [3]

$$\begin{aligned} E_{11} &= \eta_1 V_{CNT} E_{11}^{CNT} + V_m E^m \\ \frac{\eta_2}{E_{22}} &= \frac{V_{CNT}}{E_{22}^{CNT}} + \frac{V_m}{E^m} \\ \frac{\eta_3}{G_{12}} &= \frac{V_{CNT}}{G_{12}^{CNT}} + \frac{V_m}{G^m} \end{aligned} \tag{3}$$

where E_{11} and E_{22} are the Young's modulus of CNTs, respectively; and G_{12} denotes shear modulus of CNTs; E^m and G^m stand for the Young's and shear modulus of the isotropic polymer matrix, respectively. It is worth noting that it is extremely difficult to achieve the perfect bond between the CNTs and isotropic polymer matrix due to the available implicit causes such as surface effects, strain gradient effects, intermolecular coupled stress effects, etc. This leads to a decrease in a certain part

Table 1. Effective parameters of CNTs

V_{CNT}^{*}	η_1	η_2	η_3
0.11	0.149	0.934	0.934
0.14	0.150	0.941	0.941
0.17	0.140	1.381	1.381

interactive force transferred between them. Therefore, three effective parameters, i.e. $\eta_j\,(j=1,2,3)$, are suggested by Shen [3] to consider the incomplete interfacial interactions as indicated above, and given in Table 1.

Note that V_{CNT} and V_m are of the following relationship,

$$V_{CNT}+V_m=1 \tag{4}$$

Finally, the Poisson's ratio ν_{12} and the density ρ of CNTRC plate are respectively evaluated as

$$\nu_{12}=V^*_{CNT}\nu_{12}^{CNT}+V_m\nu_m \tag{5}$$

$$\rho=V_{CNT}\rho^{CNT}+V_m\rho_m \tag{6}$$

where ν_{12}^{CNT} and ρ^{CNT} are the Poisson's ratio and the density of CNTs, respectively; ν_m and ρ_m denote the Poisson's ratio and the density of the polymer matrix, respectively.

2.2. Third-order shear deformation plate theory

The displacement at a certain point through the plate thickness is computed by [19]

$$\begin{aligned}
u(x,y,z)&=u_0(x,y)-zw_{0,x}(x,y)+f(z)\beta_{0x}(x,y)\\
v(x,y,z)&=v_0(x,y)-zw_{0,y}(x,y)+f(z)\beta_{0y}(x,y)\qquad(-h/2\le z\le h/2)\\
w(x,y)&=w_0(x,y)
\end{aligned} \tag{7}$$

where $u_0, v_0, w_0, \beta_{0x}$ and β_{0y} are five unknown displacements at the middle plate of the plate; $f(z)=z-4z^3/3h^2$ is the shape function, and the subscript "," denotes the derivative.

2.3. Governing equations of motion for dynamic analysis

From Eq. (7), the strains are calculated as follows

$$\begin{aligned}
\begin{Bmatrix}\varepsilon_x\\ \varepsilon_y\\ \gamma_{xy}\end{Bmatrix}&=\begin{Bmatrix}u_{0,x}\\ v_{0,y}\\ u_{0,y}+v_{0,x}\end{Bmatrix}-z\begin{Bmatrix}w_{0b,xx}\\ w_{0b,yy}\\ 2w_{0b,xy}\end{Bmatrix}+f(z)\begin{Bmatrix}\beta_{0x,x}\\ \beta_{0y,y}\\ \beta_{0x,y}+\beta_{0y,x}\end{Bmatrix}\\
\begin{Bmatrix}\gamma_{xz}\\ \gamma_{yz}\end{Bmatrix}&=f_{,z}\begin{Bmatrix}\beta_{0x}\\ \beta_{0y}\end{Bmatrix}
\end{aligned} \tag{8}$$

Then, the stresses can be computed from the Hooke's law as follows

$$\begin{aligned}
\begin{Bmatrix}\sigma_x\\ \sigma_y\\ \tau_{xy}\end{Bmatrix}&=\begin{bmatrix}C_{11}&C_{12}&0\\ C_{21}&C_{22}&0\\ 0&0&C_{66}\end{bmatrix}\begin{Bmatrix}\varepsilon_x\\ \varepsilon_y\\ \gamma_{xy}\end{Bmatrix}\\
\begin{Bmatrix}\tau_{xz}\\ \tau_{yz}\end{Bmatrix}&=\begin{bmatrix}C_{44}&0\\ 0&C_{55}\end{bmatrix}\begin{Bmatrix}\gamma_{xz}\\ \gamma_{yz}\end{Bmatrix}
\end{aligned} \tag{9}$$

where

$$\begin{aligned}
C_{11}&=\frac{E_{11}}{1-\nu_{12}\nu_{21}},\quad C_{22}=\frac{E_{22}}{1-\nu_{12}\nu_{21}}\\
C_{12}&=C_{21}=\frac{\nu_{21}E_{11}}{1-\nu_{12}\nu_{21}},\\
C_{44}&=G_{23},\quad C_{55}=G_{13},\quad C_{66}=G_{12}
\end{aligned} \tag{10}$$

Now, the governing equations of motion for the dynamic analysis of a CNTRC plate are defined by the Hamilton's principle as follows

$$\int_0^t (\delta\Psi + \delta\Gamma - \delta\Lambda)\, dt = 0 \tag{11}$$

where $\delta\Psi$ is the virtual strain energy; $\delta\Gamma$ is the virtual work caused by the transverse loading $q(x, y, z, t)$, and $\delta\Lambda$ is the virtual kinetic energy. They are respectively given as

$$\delta\Psi = \int_{\Omega_e} \left[\left\{ \begin{array}{ccc} \delta\boldsymbol{\varepsilon}_0 & \delta\boldsymbol{\chi}_1 & \delta\boldsymbol{\chi}_2 \end{array} \right\} \mathbf{D}^{m-b} \left\{ \begin{array}{c} \boldsymbol{\varepsilon}_0 \\ \boldsymbol{\chi}_1 \\ \boldsymbol{\chi}_2 \end{array} \right\} + \left\{ \begin{array}{cc} \delta\beta_{0x} & \delta\beta_{0y} \end{array} \right\} \mathbf{D}^{s} \left\{ \begin{array}{c} \beta_{0x} \\ \beta_{0y} \end{array} \right\} \right] \mathrm{d}x\mathrm{d}y \tag{12}$$

$$\delta\Gamma = -\int_{\Omega_e} \delta w_0 q(x, y, z, t)\, \mathrm{d}x\mathrm{d}y \tag{13}$$

$$\delta\Lambda = \int_{\Omega_e} \rho \left(\dot{u}\delta\dot{u} + \dot{v}\delta\dot{v} + \dot{w}\delta\dot{w} \right) \mathrm{d}x\mathrm{d}y = -\int_{\Omega_e} \delta\mathbf{U}^T \mathbf{I}\ddot{\mathbf{U}} \mathrm{d}x\mathrm{d}y \tag{14}$$

where

$$\mathbf{D}^{m-b} = \left[\begin{array}{ccc} \mathbf{D}_1^{m-b} & \mathbf{D}_2^{m-b} & \mathbf{D}_3^{m-b} \\ \mathbf{D}_2^{m-b} & \mathbf{D}_4^{m-b} & \mathbf{D}_5^{m-b} \\ \mathbf{D}_3^{m-b} & \mathbf{D}_5^{m-b} & \mathbf{D}_6^{m-b} \end{array} \right] \tag{15}$$

$$D_{r,i,j}^{m-b} = \int_{-h/2}^{h/2} \left(1, z, z^2, f, zf, f^2\right) C_{ij} \mathrm{d}z, \quad r = 1, \ldots, 6;\ i, j = 1, 2, 6 \tag{16}$$

$$\mathbf{D}^{s} = \left[\begin{array}{cc} \displaystyle\int_{-h/2}^{h/2} g_{,z}^2 C_{44} \mathrm{d}z & 0 \\ 0 & \displaystyle\int_{-h/2}^{h/2} g_{,z}^2 C_{55} \mathrm{d}z \end{array} \right] \tag{17}$$

$$\begin{gathered} \mathbf{I} = \left[\begin{array}{ccc} \tilde{\mathbf{I}} & \mathbf{0} & \mathbf{0} \\ \mathbf{0} & \tilde{\mathbf{I}} & \mathbf{0} \\ \mathbf{0} & \mathbf{0} & \tilde{\mathbf{I}} \end{array} \right], \quad \tilde{\mathbf{I}} = \left[\begin{array}{ccc} \tilde{I}_1 & \tilde{I}_2 & \tilde{I}_4 \\ \tilde{I}_2 & \tilde{I}_3 & \tilde{I}_5 \\ \tilde{I}_4 & \tilde{I}_5 & \tilde{I}_6 \end{array} \right] \\ \left(\tilde{I}_1, \tilde{I}_2, \tilde{I}_3, \tilde{I}_4, \tilde{I}_5, \tilde{I}_6\right) = \int_{-h/2}^{h/2} \rho \left(1, z, z^2, f, zf, f^2\right) \mathrm{d}z \end{gathered} \tag{18}$$

$$\begin{gathered} \mathbf{U} = \left\{ \begin{array}{ccc} \mathbf{U}_1 & \mathbf{U}_2 & \mathbf{U}_3 \end{array} \right\}^T, \quad \mathbf{U}_1 = \left\{ \begin{array}{ccc} u_0 & -w_{0,x} & \beta_{0x} \end{array} \right\}^T \\ \mathbf{U}_2 = \left\{ \begin{array}{ccc} v_0 & -w_{0,y} & \beta_{0y} \end{array} \right\}^T, \quad \mathbf{U}_3 = \left\{ \begin{array}{ccc} w_0 & 0 & 0 \end{array} \right\}^T \end{gathered} \tag{19}$$

3. Reduced order isogeometric model

3.1. NURBS functions

The NURBS functions for a surface [20] is given by

$$N_{i,j}^{p,q}(\xi, \eta) = \frac{B_i^p(\xi) B_j^q(\eta) \omega_{i,j}}{\displaystyle\sum_{\hat{i}=1}^{n} \sum_{\hat{i}=1}^{m} B_{\hat{i}}^p(\xi) B_{\hat{j}}^q(\eta) \omega_{i,j}} \tag{20}$$

where $B_i^p(\xi)$ and $B_i^q(\eta)$ are the univariate functions of order p and q which correspond to the knot vectors of $\boldsymbol{\xi} = \left\{\xi_1, \xi_2, \ldots, \xi_i, \ldots, \xi_{n+p+1}\right\}$ and $\boldsymbol{\eta} = \left\{\eta_1, \eta_2, \ldots, \eta_i, \ldots, \eta_{m+q+1}\right\}$, respectively; and $\omega_{i,j}$ is the weight at the i-, j-th control point. And the univariate basis function $B_i^p(\xi)$ [20] as follows

$$B_i^{p=0}(\xi) = \begin{cases} 1, & \xi_i \le \xi < \xi_{i+1} \\ 0, & \text{otherwise} \end{cases} \tag{21}$$

$$B_i^{p\ge 1}(\xi) = \frac{\xi - \xi_i}{\xi_{i+p} - \xi_i} B_i^{p-1}(\xi) + \frac{\xi_{i+p+1} - \xi}{\xi_{i+p+1} - \xi_{i+1}} B_{i+1}^{p-1}(\xi) \tag{22}$$

where $\xi_i \in \mathbb{R}$ is the i-th knot in the parameter space $\boldsymbol{\xi}$; i the knot index; p and n are the polynomial order and the number of functions, respectively.

3.2. Isogeometric analysis

For the free vibration analysis with the harmonic motion, i.e. $\ddot{\mathbf{U}} = -\omega^2\mathbf{U}$, the full IGA model is established from Eq. (11) as follows

$$\left(\mathbf{K} - \omega^2\mathbf{M}\right)\mathbf{U} = \mathbf{0} \tag{23}$$

where $\boldsymbol{\omega}$ is the eigenvalue vector; the global stiffness matrix $\mathbf{K}$ and the mass matrix $\mathbf{M}$ are respectively defined as follows

$$\mathbf{K} = \int_{\Omega^e} \sum_{i=1}^{m\times n} \left[\begin{pmatrix} \boldsymbol{\Theta}_i^m & \boldsymbol{\Theta}_i^{b1} & \boldsymbol{\Theta}_i^{b2} \end{pmatrix} \mathbf{D}^{m-b} \begin{Bmatrix} \boldsymbol{\Theta}_i^m \\ \boldsymbol{\Theta}_i^{b1} \\ \boldsymbol{\Theta}_i^{b2} \end{Bmatrix} + \left(\boldsymbol{\Theta}_i^s\right)^T \mathbf{D}^s \boldsymbol{\Theta}_i^s \right] \mathrm{d}x\mathrm{d}y \tag{24}$$

$$\mathbf{M} = \int_{\Omega^e} \sum_{i=1}^{m\times n} \boldsymbol{\Lambda}^T \mathbf{m} \boldsymbol{\Lambda} \mathrm{d}x\mathrm{d}y \tag{25}$$

where

$$\begin{aligned} \boldsymbol{\Theta}_i^m &= \begin{bmatrix} N_{i,x} & 0 & 0 & 0 & 0 \\ 0 & N_{i,y} & 0 & 0 & 0 \\ N_{i,y} & N_{i,x} & 0 & 0 & 0 \end{bmatrix}, \quad \boldsymbol{\Theta}_i^{b1} = -\begin{bmatrix} 0 & 0 & -N_{i,xx} & 0 & 0 \\ 0 & 0 & -N_{i,yy} & 0 & 0 \\ 0 & 0 & -2N_{i,xy} & 0 & 0 \end{bmatrix} \\ \boldsymbol{\Theta}_i^{b2} &= \begin{bmatrix} 0 & 0 & 0 & N_{i,x} & 0 \\ 0 & 0 & 0 & 0 & N_{i,y} \\ 0 & 0 & 0 & N_{i,y} & N_{i,x} \end{bmatrix}, \quad \boldsymbol{\Theta}_i^s = \begin{bmatrix} 0 & 0 & 0 & N_i & 0 \\ 0 & 0 & 0 & 0 & N_i \end{bmatrix} \end{aligned} \tag{26}$$

$$\begin{aligned} \boldsymbol{\Lambda} &= \begin{Bmatrix} \boldsymbol{\Lambda}_1 & \boldsymbol{\Lambda}_2 & \boldsymbol{\Lambda}_3 \end{Bmatrix}^T, \quad \boldsymbol{\Lambda}_1 = \begin{bmatrix} N_i & 0 & 0 & 0 & 0 \\ 0 & 0 & -N_{i,x} & 0 & 0 \\ 0 & 0 & 0 & N_i & 0 \end{bmatrix} \\ \boldsymbol{\Lambda}_2 &= \begin{bmatrix} 0 & N_i & 0 & 0 & 0 \\ 0 & 0 & -N_{i,y} & 0 & 0 \\ 0 & 0 & 0 & 0 & N_i \end{bmatrix}, \quad \boldsymbol{\Lambda}_3 = \begin{bmatrix} 0 & 0 & N_I & 0 & 0 \\ 0 & 0 & 0 & 0 & 0 \\ 0 & 0 & 0 & 0 & 0 \end{bmatrix} \end{aligned} \tag{27}$$

with N_i being the i-th NURBS function.

From Eq. (11), the full IGA model for the dynamic analysis is expressed as follows

$$\mathbf{M}\ddot{\mathbf{U}} + \mathbf{K}\mathbf{U} = \mathbf{F}(t) \tag{28}$$

where the load vector is given by

$$\mathbf{F}(t) = \int_{\Omega^e} \sum_{i=1}^{m\times n} \begin{Bmatrix} 0 & 0 & N_i & 0 & 0 \end{Bmatrix}^T q(x, y, z, t)\, \mathrm{d}x\mathrm{d}y \tag{29}$$

3.3. Second-order Neumann series expansion

Let the subscript "m" be the DOFs used to build the ROM, and the subscript "s" be the remaining DOFs. Then, Eq. (23) can be separated as follows

$$\begin{bmatrix} \mathbf{K}_{mm} & \mathbf{K}_{ms} \\ \mathbf{K}_{sm} & \mathbf{K}_{ss} \end{bmatrix} \begin{Bmatrix} \mathbf{\Phi}_m \\ \mathbf{\Phi}_s \end{Bmatrix} = \omega^2 \begin{bmatrix} \mathbf{M}_{mm} & \mathbf{M}_{ms} \\ \mathbf{M}_{sm} & \mathbf{M}_{ss} \end{bmatrix} \begin{Bmatrix} \mathbf{\Phi}_m \\ \mathbf{\Phi}_s \end{Bmatrix} \tag{30}$$

In comparison with the Guyan's method and the first-order Neumann series expansion which were suggested by Yang [18], the second-order Neumann series expansion is more accurate than the others, it is hence adopted in this study. According to the second-order Neumann series expansion, Eq. (30) can be rewritten in terms of the model order reduction as follows

$$\mathbf{K}_{ROM}\mathbf{\Phi}_m = \omega_{ROM}^2 \mathbf{M}_{ROM}\mathbf{\Phi}_m \tag{31}$$

where ω_{ROM} is the eigenvector attained by the ROM; $\mathbf{K}_{ROM}$ and $\mathbf{M}_{ROM}$ are the reduced order global stiffness and lumped mass matrices, respectively. And they are calculated by

$$\mathbf{K}_{ROM} = \mathbf{V}^T\mathbf{K}\mathbf{V}, \quad \mathbf{M}_{ROM} = \mathbf{V}^T\mathbf{M}\mathbf{V} \tag{32}$$

where $\mathbf{V}$ is the matrix employed to transform a system from a large domain into a smaller space, given by

$$\mathbf{V} = \begin{bmatrix} \mathbf{I}_{mm} \\ -\left[\mathbf{b}_1 + \mathbf{K}_{ss}^{-1}\mathbf{M}_{ss}\left(\mathbf{a}_1\mathbf{a}_4 + \mathbf{a}_1\mathbf{a}_5\right)\right]^{-1}\left[\mathbf{b}_2 + \mathbf{K}_{ss}^{-1}\mathbf{M}_{ss}\left(\mathbf{a}_1\mathbf{a}_2 + \mathbf{a}_1\mathbf{a}_3\right)\right] \end{bmatrix} \tag{33}$$

where

$$\begin{aligned} \mathbf{a}_1 &= \mathbf{K}_{ss}^{-1}\mathbf{M}_{ss}\mathbf{K}_{ss}^{-1}\mathbf{K}_{sm}\mathbf{M}_{mm}^{-1} \\ \mathbf{a}_2 &= \mathbf{K}_{mm}\mathbf{M}_{mm}^{-1}\mathbf{K}_{mm} \\ \mathbf{a}_3 &= \mathbf{K}_{ms}\mathbf{M}_{ss}^{-1}\mathbf{K}_{sm} \\ \mathbf{a}_4 &= \mathbf{K}_{mm}\mathbf{M}_{mm}^{-1}\mathbf{K}_{ms} \\ \mathbf{a}_5 &= \mathbf{K}_{ms}\mathbf{M}_{ss}^{-1}\mathbf{K}_{ss} \end{aligned} \tag{34}$$

$$\begin{aligned} \mathbf{b}_1 &= \mathbf{I}_{ss} + \mathbf{A}_1\mathbf{K}_{ms} \\ \mathbf{b}_2 &= \mathbf{K}_{ss}^{-1}\mathbf{K}_{sm} + \mathbf{A}_1\mathbf{K}_{mm} \end{aligned} \tag{35}$$

The i-th eigenvector corresponding to the remaining DOFs "s" can be inferred by

$$\mathbf{\Phi}_{s,i} = -\left[\mathbf{b}_1 + \mathbf{K}_{ss}^{-1}\mathbf{M}_{ss}\left(\mathbf{a}_1\mathbf{a}_4 + \mathbf{a}_1\mathbf{a}_5\right)\right]^{-1}\left[\mathbf{b}_2 + \mathbf{K}_{ss}^{-1}\mathbf{M}_{ss}\left(\mathbf{a}_1\mathbf{a}_2 + \mathbf{a}_1\mathbf{a}_3\right)\right]\mathbf{\Phi}_{m,i} \tag{36}$$

Now, the reduced IGA model for the dynamic analysis is given by

$$\mathbf{M}_{ROM}\ddot{\mathbf{U}} + \mathbf{K}_{ROM}\mathbf{U} = \mathbf{F}_{ROM}(t) \tag{37}$$

with

$$\mathbf{F}_{ROM}(t) = \mathbf{V}^T\mathbf{F}(t) \tag{38}$$

In this study, the Newmark approach with the assumption of the average acceleration is utilized to resolve Eq. (37).

4. Numerical examples

4.1. Free vibration

In this example, a square CNTRC plate is investigated. This problem was before studied by Zhu et al. [2] using the standard FEM based on the first order shear deformation plate theory. The matrix is of the material properties as follows: E^m = 2.1 GPa, ν_m = 0.34, ρ_m = 1160 kg/m^3. Meanwhile, the material features of CNTs at the temperature 300 K are: E_{11}^{CNT} = 5.6466 TPa, E_{22}^{CNT} = 7.08 TPa, G_{12}^{CNT} = 1.9445 TPa, ν_{12}^{CNT} = 0.175, ρ^{CNT} = 1400 kg/m^3, and $G_{23} = G_{13} = G_{12}$. The plate thickness h is 2 mm, while the edge-to-thickness ratios (a/h) are investigated with 10, 20 and 50. For comparison with the previously published results, the frequencies are normalized by the following formula, i.e. $\bar{\omega} = \dfrac{\omega a^2}{h}\sqrt{\dfrac{\rho^m}{E^m}}$. All edges of the square plate are restricted as the simply supported boundary which is symboled as 'S'. After very careful investigations of the convergence of discretized meshes, a uniform mesh of 7×7 cubic NURBS elements is sufficient to achieve acceptable accuracy for the obtained results. Tables 2, 3 and 4 report outcomes for various kinds of CNT distributions and different ratios of a/h. It can be found that the results obtained by the full IGA are in good agreement with those of the reference solutions.

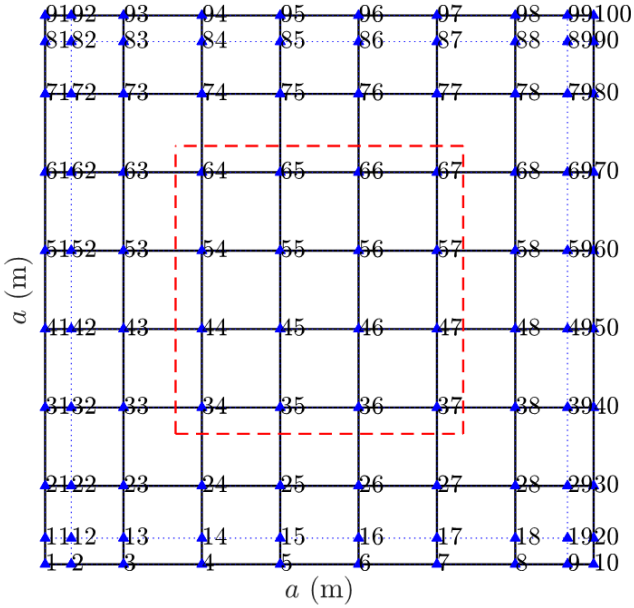

Figure 2. Control points of the SSSS-CNTRC square plate

Now, the ability of the reduced order IGA developed in this work is illustrated. For that aim, only DOFs attached to control points marked in a red rectangle with dashed lines as plotted in Fig. 2 are taken into account. According to this selection, there are a total of 64 DOFs used to establish a reduced order model. As a consequence, the number of DOFs in the reduced IGA reduces 20% against that of the full model. Currently, the DOFs selected to build the MOR-based IGA are mainly based on the characteristics of free vibration of the investigated problem without optimization. In the next studies, they are optimized to achieve the best MOR. As can seen from Tables 2, 3 and 4, the results provided by the reduced IGA agree with those of the full model as well as the other study. This confirms the reliability and efficiency of the proposed IGA which is built by reducing the dimensionality of the plate model.

Table 2. The non-dimensional natural frequencies of the SSSS-CNTRC square plate with $V^*_{CNT} = 0.11$

a/h	Mode	U			V			O			X		
		Ref. [2]	This study		Ref. [2]	This study		Ref. [2]	This study		Ref. [2]	This study	
			Full IGA	Reduced IGA		Full IGA	Reduced IGA		Full IGA	Reduced IGA		Full IGA	Reduced IGA
10	1	13.532	13.610	13.611	12.452	12.518	12.518	11.550	11.407	11.407	14.616	14.740	14.741
	2	17.700	17.705	17.708	17.060	17.061	17.064	16.265	16.156	16.159	18.646	18.641	18.645
	3	19.449	19.428	19.430	19.499	19.477	19.479	19.499	19.477	19.479	19.499	19.478	19.480
	4	19.449	19.428	19.440	19.499	19.477	19.490	19.499	19.477	19.489	19.499	19.478	19.490
	5	27.569	26.941	26.946	27.340	26.716	26.721	26.513	25.958	25.964	28.519	27.734	27.739
20	1	17.355	17.340	17.342	15.110	15.098	15.099	13.523	13.434	13.434	19.939	19.941	19.943
	2	21.511	21.457	21.460	19.903	19.855	19.858	18.486	18.391	18.393	23.776	23.721	23.724
	3	32.399	31.983	31.985	31.561	31.150	31.152	30.166	29.763	29.765	34.389	33.928	33.930
	4	38.898	38.855	38.859	38.998	38.955	38.959	38.998	38.953	38.958	38.998	38.955	38.960
	5	38.898	38.855	38.879	38.998	38.955	38.980	38.998	38.953	38.977	38.998	38.955	38.979
50	1	19.223	19.161	19.161	16.252	16.206	16.206	14.302	14.253	14.253	22.984	22.905	22.906
	2	23.408	23.283	23.283	21.142	21.038	21.038	19.373	19.277	19.277	26.784	26.631	26.631
	3	34.669	34.119	34.120	33.350	32.818	32.818	31.615	31.110	31.111	37.591	37.000	37.000
	4	54.043	52.443	52.443	53.430	51.854	51.854	51.370	49.862	49.863	56.946	55.263	55.263
	5	70.811	70.129	70.130	60.188	59.606	59.608	53.035	52.265	52.267	83.150	81.804	81.807

Table 3. The non-dimensional natural frequencies of the SSSS-CNTRC square plate with $V^*_{CNT} = 0.14$

a/h	Mode	U			V			O			X		
		Ref. [2]	This study		Ref. [2]	This study		Ref. [2]	This study		Ref. [2]	This study	
			Full IGA	Reduced IGA		Full IGA	Reduced IGA		Full IGA	Reduced IGA		Full IGA	Reduced IGA
10	1	14.306	14.415	14.416	13.256	13.343	13.343	12.338	12.202	12.202	15.368	15.458	15.459
	2	18.362	18.395	18.398	17.734	17.753	17.756	16.848	16.755	16.758	19.385	19.345	19.348
	3	19.791	19.774	19.776	19.879	19.862	19.864	19.879	19.862	19.864	19.879	19.863	19.865
	4	19.791	19.774	19.786	19.879	19.862	19.876	19.879	19.862	19.874	19.879	19.863	19.875
	5	28.230	27.613	27.618	28.021	27.399	27.404	27.003	26.489	26.494	29.398	28.532	28.537
20	1	18.921	18.936	18.938	16.510	16.520	16.522	14.784	14.705	14.706	21.642	21.629	21.630
	2	22.867	22.844	22.847	21.087	21.063	21.067	19.462	19.385	19.386	25.360	25.290	25.294
	3	33.570	33.182	33.185	32.617	32.229	32.232	30.906	30.532	30.533	35.938	35.457	35.460
	4	39.583	39.549	39.553	39.759	39.725	39.730	39.759	39.724	39.728	39.759	39.727	39.731
	5	39.583	39.549	39.573	39.759	39.725	39.750	39.759	39.724	39.748	39.759	39.727	39.751
50	1	21.354	21.323	21.324	17.995	17.975	17.975	15.801	15.773	15.773	25.555	25.501	25.501
	2	25.295	25.201	25.201	22.643	22.566	22.566	20.563	20.492	20.492	29.192	29.060	29.060
	3	36.267	35.749	35.749	34.660	34.156	34.156	32.509	32.034	32.034	39.833	39.257	39.258
	4	55.608	54.025	54.025	54.833	53.275	53.276	52.184	50.703	50.703	59.333	57.641	57.641
	5	78.110	77.511	77.513	66.552	66.025	66.027	58.748	57.991	57.993	87.814	84.676	84.678

Table 4. The non-dimensional natural frequencies of the SSSS-CNTRC square plate with $V^*_{CNT} = 0.17$

a/h	Mode	U			V			O			X		
		Ref. [2]	This study		Ref. [2]	This study		Ref. [2]	This study		Ref. [2]	This study	
			Full IGA	Reduced IGA		Full IGA	Reduced IGA		Full IGA	Reduced IGA		Full IGA	Reduced IGA
10	1	16.815	16.687	16.688	15.461	15.296	15.297	14.282	13.962	13.963	18.278	18.050	18.051
	2	22.063	21.919	21.923	21.307	21.158	21.161	20.091	19.917	19.920	23.541	23.216	23.220
	3	24.337	24.308	24.310	24.511	24.480	24.483	24.512	24.479	24.482	24.512	24.482	24.485
	4	24.337	24.308	24.323	24.511	24.480	24.497	24.512	24.479	24.495	24.512	24.482	24.497
	5	34.448	33.584	33.590	34.273	33.416	33.422	32.766	32.174	32.182	36.245	34.931	34.937
20	1	21.456	20.965	20.967	18.638	18.202	18.204	16.628	16.186	16.186	24.764	24.140	24.142
	2	26.706	26.274	26.277	24.734	24.381	24.385	22.739	22.420	22.421	29.819	29.216	29.221
	3	40.401	39.650	39.652	39.471	38.798	38.801	37.139	36.581	36.582	43.612	42.618	42.621
	4	48.674	48.615	48.621	49.023	48.962	48.967	49.024	48.959	48.964	49.024	48.964	48.969
	5	48.674	48.615	48.646	49.023	48.962	48.994	49.024	48.959	48.989	49.024	48.964	48.994
50	1	23.697	22.980	22.980	19.982	19.410	19.411	17.544	17.052	17.052	28.413	27.511	27.511
	2	28.987	28.312	28.313	26.204	25.698	25.699	23.783	23.375	23.375	33.434	32.540	32.540
	3	43.165	42.129	42.129	41.646	40.765	40.765	38.855	38.096	38.097	47.547	46.267	46.267
	4	67.475	65.247	65.247	66.943	64.870	64.871	63.179	61.293	61.294	72.570	70.028	70.028
	5	87.385	84.317	84.319	74.030	71.372	71.374	65.154	62.595	62.596	102.939	99.251	99.254

4.2. Dynamic analysis

In this part, the dynamic behavior of the SSSS-CNTRC plate with $a/h = 10$ is presented. A uniform loading of $q(t) = 10$ N/cm^2 is applied to the plate. The time-history displacement at the plate center is analyzed in the time domain [0, 300] μ sec with the time step $\Delta t = 1$ μ sec. This case uses the same number of NURBS elements as that of the previous example. Figs. 3, 4 and 5 show the deflection at the plate center for four different configurations of CNT distributions concerning $V^*_{CNT} = 0.11, 0.14$ and 0.17 attained by the full IGA and reduced IGA, respectively. It can be found from the above figures that the ROM-based IGA can yield outcomes with high compatibility compared with the full model. Additionally, the CNT distribution with the X-type configuration always gives the largest stiffness. This can be recognized via the smallest deflection obtained in all investigated cases as shown in Figs. 6, 7 and 8. The reason is CNTs are put far away from the neutral plane. Accordingly, the moment of inertia becomes larger and the bending stiffness is also better.

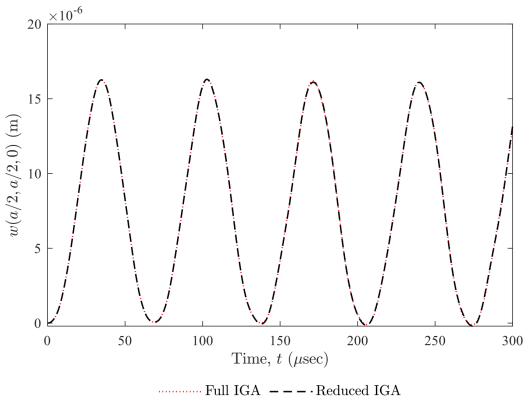

(a) U-type

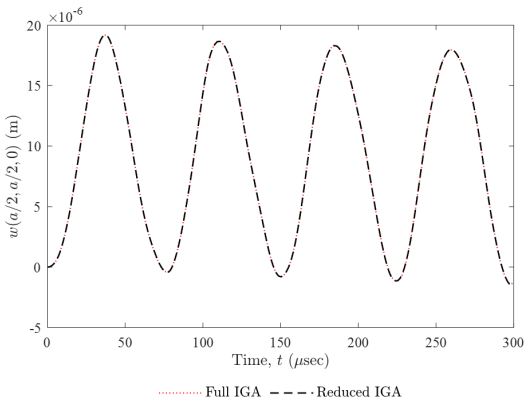

(b) V-type

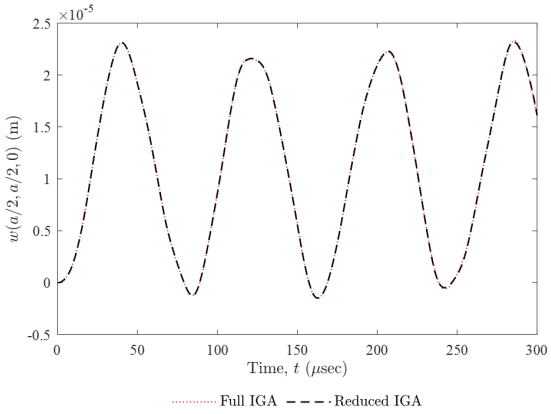

(c) O-type

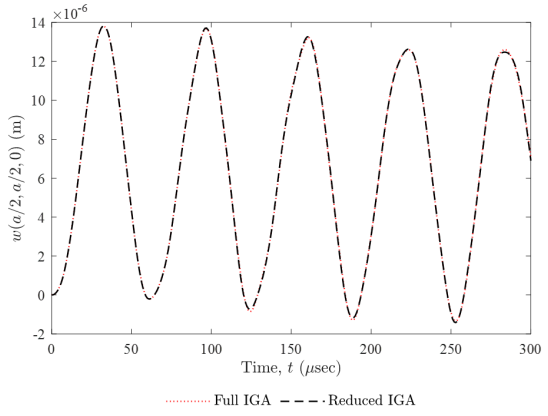

(d) X-type

Figure 3. The deflection at the plate center for four different configurations of CNT distributions with $V^*_{CNT} = 0.11$

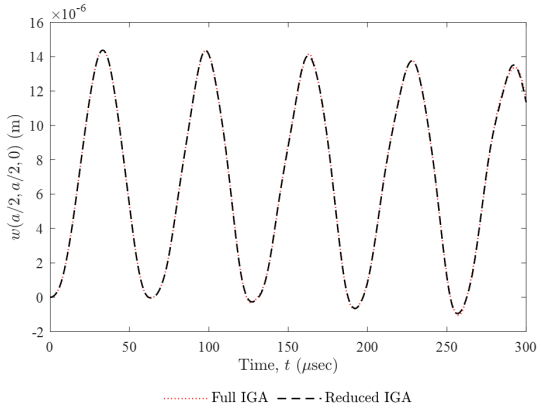

(a) U-type

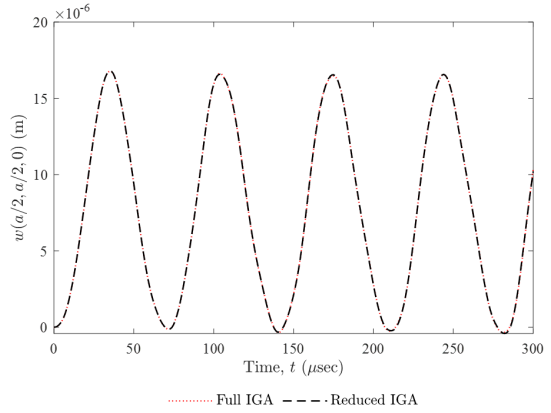

(b) V-type

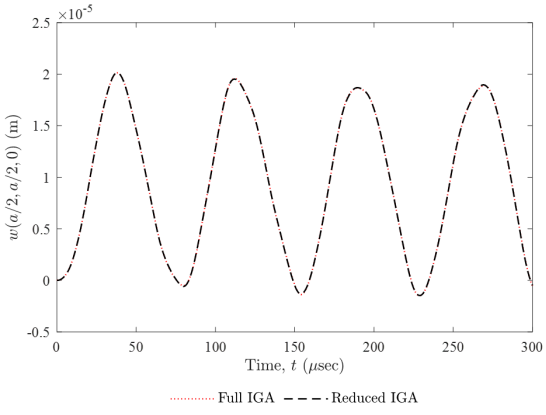

(c) O-type

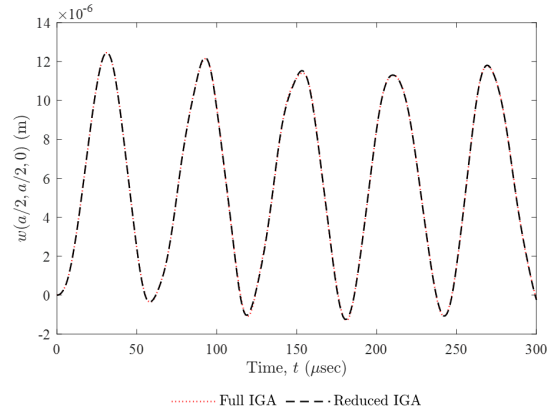

(d) X-type

Figure 4. The deflection at the plate center for four different configurations of CNT distributions with $V^*_{CNT} = 0.14$

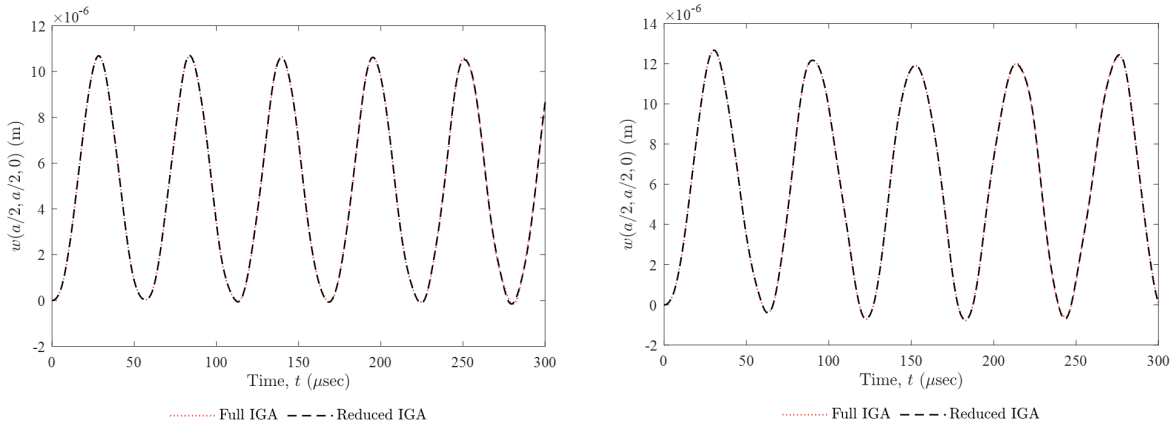

(a) U-type

(b) V-type

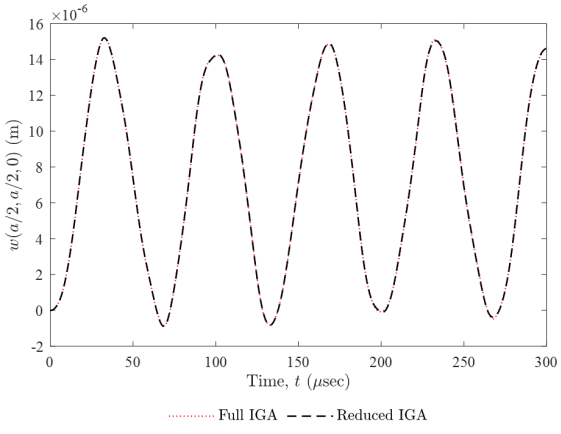

(c) O-type

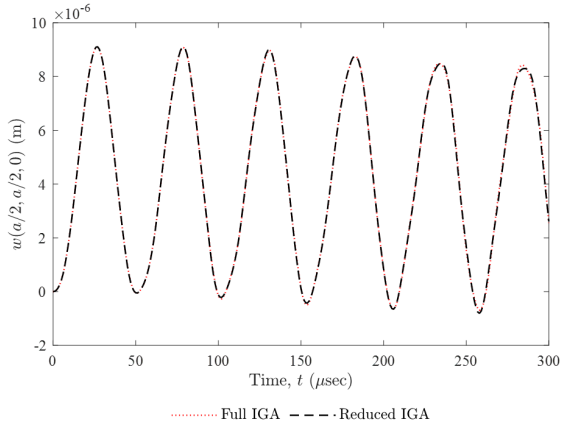

(d) X-type

Figure 5. The deflection at the plate center for four different configurations of CNT distributions with $V^*_{CNT} = 0.17$

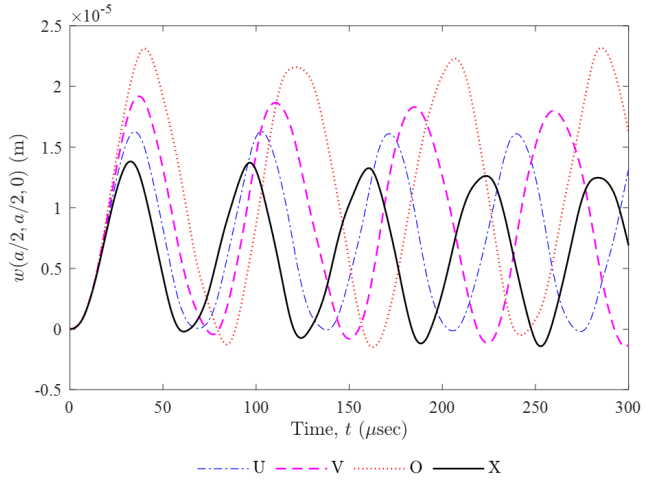

Figure 6. Comparison of the deflection at the plate center for four different configurations of CNT distributions with $V^*_{CNT} = 0.11$ attained by the reduced IGA

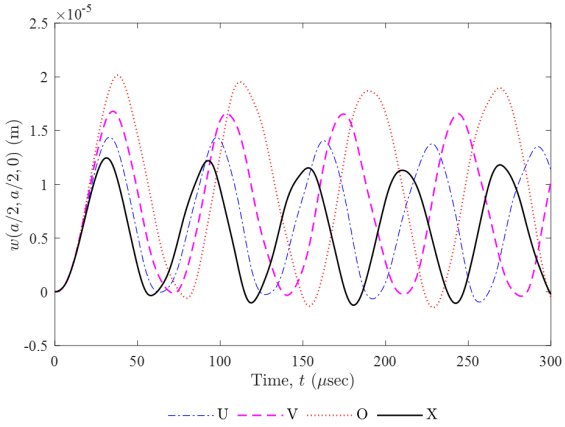

Figure 7. Comparison of the deflection at the plate center for four different configurations of CNT distributions with $V^*_{CNT} = 0.14$ attained by the reduced IGA

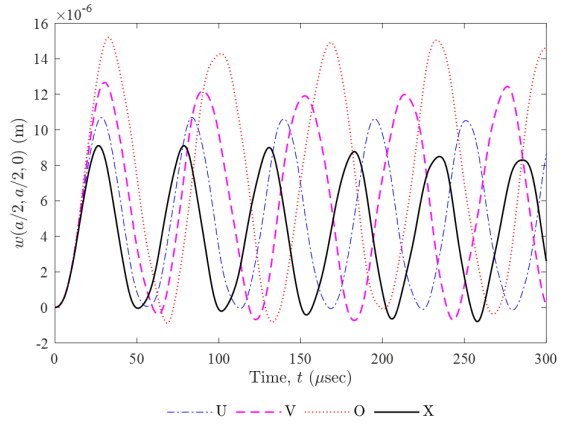

Figure 8. Comparison of the deflection at the plate center for four different configurations of CNT distributions with $V^*_{CNT} = 0.17$ attained by the reduced IGA

5. Conclusions

In this paper, the transient responses of CNTRC plates are analyzed by the so-called reduced IGA for the first time. In this paradigm, only important DOFs defined at control points within the IGA framework are utilized to construct the order reduction of the isogeometric model based on the second-order Neumann series expansion. The dynamic equation system of the CNTRC plate in the ROM is resolved by the Newmark method. Then, the remaining DOFs of the structural system can be numerically inferred by the mathematical expressions derived in the ROM. Four different configurations of the distribution of CNTs in the plate are investigated. Several examples are demonstrated to confirm the reliability of the reduced IGA with full model and other publications. Acquired outcomes indicated that the X-type configuration is of the time-history responses with the smallest amplitude. This proves that this CNT distribution is the best against the others. In the next studies, optimization of selecting important DOFs as well as distributing the CNTs is interesting and will be soon carried out.

6. Acknowledgements

This research is funded by Vietnam National University Ho Chi Minh City (VNU-HCM) under Grant No. B2024-20-12: “Modelling and dynamic analysis of thick plates used in civil engineering structures”.

References

[1] Rafiee, M., Yang, J., Kitipornchai, S. (2013). Large amplitude vibration of carbon nanotube reinforced functionally graded composite beams with piezoelectric layers. *Composite Structures*, 96:716–725.

[2] Zhu, P., Lei, Z. X., Liew, K. M. (2012). Static and free vibration analyses of carbon nanotube-reinforced composite plates using finite element method with first order shear deformation plate theory. *Composite Structures*, 94(4):1450–1460.

[3] Shen, H.-S. (2009). Nonlinear bending of functionally graded carbon nanotube-reinforced composite plates in thermal environments. *Composite Structures*, 91(1):9–19.

[4] Mallek, H., Mellouli, H., Said, L. B., Wali, M., Dammak, F., Boujelbene, M. (2023). Bending and free vibration analyses of CNTRC shell structures considering agglomeration effects with through-the-thickness stretch. *Thin-Walled Structures*, 191:111036.

[5] Soni, S. K., Thomas, B., Swain, A., Roy, T. (2022). Functionally graded carbon nanotubes reinforced composite structures: An extensive review. *Composite Structures*, 299:116075.

[6] Hughes, T. J. R., Cottrell, J. A., Bazilevs, Y. (2005). Isogeometric analysis: CAD, finite elements, NURBS, exact geometry and mesh refinement. *Computer Methods in Applied Mechanics and Engineering*, 194(39–41):4135–4195.

[7] Phung-Van, P., Lieu, Q. X., Nguyen-Xuan, H., Abdel Wahab, M. (2017). Size-dependent isogeometric analysis of functionally graded carbon nanotube-reinforced composite nanoplates. *Composite Structures*, 166:120–135.

[8] Farzam, A., Hassani, B. (2018). Thermal and mechanical buckling analysis of FG carbon nanotube reinforced composite plates using modified couple stress theory and isogeometric approach. *Composite Structures*, 206:774–790.

[9] Nguyen, L. B., Viet, T. B., Nguyen, H.-Y. (2021). An isogeometric formulation with a three-variable high order shear deformation theory for free vibration analysis of FG porous plates reinforced by graphene platelets. *Journal of Science and Technology in Civil Engineering (STCE) - NUCE*, 15(2):51–66.

[10] Do, D. T. T., Thai, S. (2023). Transient analysis of functionally graded plates using extreme gradient boosting. *Journal of Science and Technology in Civil Engineering (STCE) - HUCE*, 17(4):26–36.

[11] Phung-Van, P., Thanh, C.-L., Nguyen-Xuan, H., Abdel-Wahab, M. (2018). Nonlinear transient isogeometric analysis of FG-CNTRC nanoplates in thermal environments. *Composite Structures*, 201:882–892.

[12] Nguyen-Quang, K., Vo-Duy, T., Dang-Trung, H., Nguyen-Thoi, T. (2018). An isogeometric approach for dynamic response of laminated FG-CNT reinforced composite plates integrated with piezoelectric layers. *Computer Methods in Applied Mechanics and Engineering*, 332:25–46.

[13] Van Do, V. N., Jeon, J.-T., Lee, C.-H. (2020). Dynamic analysis of carbon nanotube reinforced composite plates by using Bézier extraction based isogeometric finite element combined with higher-order shear deformation theory. *Mechanics of Materials*, 142:103307.

[14] Thai, C. H., Nguyen-Xuan, H. (2020). A simple size-dependent isogeometric approach for bending analysis of functionally graded microplates using the modified strain gradient elasticity theory. *Vietnam Journal of Mechanics*, 42(3):255–267.

[15] Dang, K. D., Nguyen, N. H., Lee, S., Luong, V. H., Le, T. A., Lieu, Q. X. (2023). A novel model order reduction-based two-stage damage detection paradigm for trusses using time–history acceleration. *Advances in Engineering Software*, 176:103374.

[16] Lieu, Q. X. (2023). A novel multistage damage detection method for trusses using time-history data based on model order reduction and deep neural network. *Mechanical Systems and Signal Processing*, 200:110635.

[17] Qui, L. X. (2023). Damage identification of trusses using limited modal features and ensemble learning. *Journal of Science and Technology in Civil Engineering (STCE) - HUCE*, 17(2):9–20.

[18] Yang, Q. W. (2009). Model reduction by Neumann series expansion. *Applied Mathematical Modelling*, 33(12):4431–4434.

[19] Reddy, J. (2000). Analysis of functionally graded plates. *International Journal for Numerical Methods in Engineering*, 47(1-3):663–684.

[20] de Boor, C. (1972). On calculating with B-splines. *Journal of Approximation Theory*, 6(1):50–62.